FADE-IN CONTROL FOR FEEDBACK DELAY NETWORKS

Nils Meyer-Kahlen[1], *Sebastian J. Schlecht*[1,2] *and Tapio Lokki*[1]

[1]Acoustics Lab, Dept. of Signal Processing and Acoustics
[2]Media Lab, Dept. of Media
Aalto University
Espoo, Finland
nils.meyer-kahlen@aalto.fi

ABSTRACT

In virtual acoustics, it is common to simulate the early part of a Room Impulse Response using approaches from geometrical acoustics and the late part using Feedback Delay Networks (FDNs). In order to transition from the early to the late part, it is useful to slowly fade-in the FDN response. We propose two methods to control the fade-in, one based on double decays and the other based on modal beating. We use modal analysis to explain the two concepts for incorporating this fade-in behaviour entirely within the IIR structure of a multiple input multiple output FDN. We present design equations, which allow for placing the fade-in time at an arbitrary point within its derived limit.

1. INTRODUCTION

Convolution reverbs in the Ambisonics or the binaural domain are well suited for accurately auralizing measured rooms. Albeit the existence of fast convolution techniques, the computational effort of convolving a signal with a several second long impulse responses (IR) is very high, especially in multichannel scenarios. To cope with this, hybrid reverbs have been introduced, e.g. [1]. In such systems, convolution is only used for the early part of the IR, obtained by measurement or simulation, while the late part is synthesized using an IIR filter structure. These can be generalized by feedback delay networks (FDNs), see [2] for an overview of different techniques. Methods exist for matching the parameters of the early and late part of the responses [3]. This hybrid concept is especially advantageous, when turning towards 6 degrees of freedom audio rendering. In this case, early reflections up to a certain reflection order can be computed dynamically using the Image Source Method (ISM) [4], and the late part can be synthesized using a Feedback Delay Network. In one possible framework, e.g. as used in [5], the ISM stage encodes the reflections in higher order Ambisonics (HOA) along with the direct sound. The ISM may include source directivity and reflection filters and can be updated in real-time. For synthesizing the late part of the impulse response response in such spatial audio applications, it is advantageous to use a multiple input multiple output (MIMO) FDN. An example of the components in a hybrid reverb is shown in Figure 1.

To avoid adding energy to the well designed and possibly adaptive first part of the response, the early part of the FDN's response should be removed. The simplest idea is to apply a window function, which serves the purpose [6], but is only possible if the FDN output is pre-rendered and used in a convolver. This conflicts with the motivation for using the FDN as an efficient IIR structure in the first place. Another method is to add a phase inverted version of the undesired part of the FDN response to the early, convolutional part of the response [7]. Arbitrary fade-in behaviour can be realized by windowing this part, but the length of the convolution might be increased. Also, the simulated reflections might be sparse in nature, which makes time-domain convolution of the reflections efficient. This property is lost when using this convolutional fade-in approach. We demonstrate IIR based fade-in in a basic MIMO network. Such a network, as implemented in the FDNReverb[1], can for example be used as a send effect in Ambisonics [8]. In this MIMO case, the presented IIR fade-in approach is especially beneficial, as convolutional fade-in cancellation would need to be done for every input-output pair.

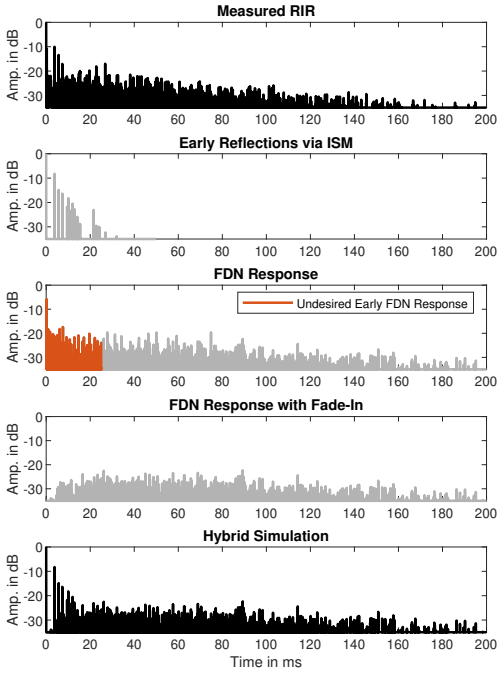

Figure 1: Example for hybrid reverberation using the Image Source Method for the early part, and a Feedback Delay Network for the late part of the response. Fade-in allows for cancelling the FDN's early response. The modelled room is the variable acoustics chamber at the Aalto Acoustics Lab.

[1]https://plugins.iem.at/

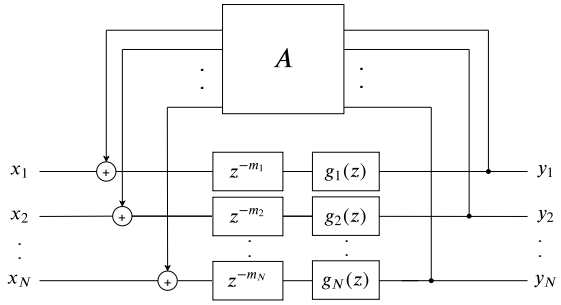

Figure 2: MIMO Feedback Delay Network, where $\boldsymbol{A}$ symbolizes the feedback-matrix, z^{-m_i} indicate delays and $g_i(z)$ attenuation filters.

To obtain an FDN with fade-in that is entirely implemented within the IIR structure, the output of a second networks with similar parameters can be subtracted from the first. The double decay idea of using a second network with faster decay has been introduced in [9] and [10], and was applied in [11], but no comprehensive description of how the network parameters should be chosen in order to achieve a specific fade-in time exists so far. The second novelty here is based on applying a small rotation to the feedback matrix resulting in modal beating. We use modal analysis to examine examples of both techniques using the FDN toolbox [12]. All plots are reproducible with the provided Matlab code [2].

2. MULTICHANNEL FDN

The transfer function of the FDN shown in Figure 2 is given by

$$\boldsymbol{H}(z) = [\boldsymbol{D_m}(z)^{-1} - \boldsymbol{A}]^{-1}, \tag{1}$$

where $\boldsymbol{D_m}(z) = \mathrm{diag}\big(g_1(z)z^{-m_1}, \ldots, g_N(z)z^{-m_N}\big)$ contains delays with the lengths $\boldsymbol{m}$ in samples on rate f_s and attenuation filters $g_i(z)$. The transfer function from every input to every output can be decomposed into a sum of $\mathfrak{N}$ one-pole resonators, called modes of the network [13]

$$\boldsymbol{H}(z) = \sum_{i=1}^{\mathfrak{N}} \frac{\boldsymbol{\rho}_i}{1 - \lambda_i\, z^{-1}}. \tag{2}$$

The time response of each mode is given by

$$\boldsymbol{h}_i(t) = \boldsymbol{\rho}_i \lambda_i^t = |\boldsymbol{\rho}_i||\lambda_i|^t e^{\imath(\omega_i t + \angle \boldsymbol{\rho}_i)} \tag{3}$$

In this representation, where t is the discrete time variable and $\imath$ is the imaginary unit, it becomes apparent how the pole-angles $\omega_i = \angle\lambda_i$ represent the frequency of the mode, and the pole-radius $|\lambda_i|$ determines its decay time. Only the amplitudes $|\boldsymbol{\rho}_i|$ and phases $\angle\boldsymbol{\rho}_i$ of the residues are different for every input-output pair of the MIMO FDN. Thus, the dynamic behavior is solely dependent on the poles such that it is sufficient to focus on the single input single output case to study the fade-in control.

We now define the time constant τ_i of every modal decay, such that

$$|\lambda_i|^t = e^{-\frac{t}{\tau_i}} \quad \text{with} \quad \tau_i = \frac{-1}{\log|\lambda_i|}. \tag{4}$$

[2] https://version.aalto.fi/gitlab/soundinvr_public/fadefdn

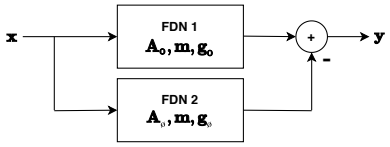

Figure 3: 2 FDNs. The output of the second network with slightly modified parameters $\boldsymbol{A}_\emptyset, g_\emptyset$ is subtracted from the first.

This formulation helps to relate the modal decay to the reverberation time T_{60}, which is defined as the time it takes for a system to reach -60 dB of it's initial energy. The time constant τ_i of the exponential decay of each mode is related to T_{60} by

$$\tau_i = -\frac{T_{60}(\omega_i) f_s}{\log\left(10^{-\frac{60}{20}}\right)} \approx \frac{T_{60}(\omega_i) f_s}{6.9078}. \tag{5}$$

If the feedback matrix is chosen to be lossless, the reverberation time T_{60} can be controlled by simply modifying the gain introduced in the feedback paths. When assuming that the introduced filters' phase delay is small against the delay elements' length m_i, the required gain in dB is determined by

$$|g_i(e^{\imath\omega})| = -60\frac{m_i}{f_s T_{60}(\omega)}. \tag{6}$$

3. FADE-IN CONTROL

To achieve the desired fade-in behaviour, the output of a second, phase-inverted network is added to the first, see Fig. 3. The parameters of the second network will undergo a slight modification, which is either based on changing the gains in the feedback paths, as described in the next section, or on applying a small rotation to the feedback matrix, which is shown in section 3.3.

3.1. Double Decay

The first way of modifying the second network is to change the gains in the feedback paths, in order to obtain a faster decay of the second network ø compared to the first ($\tau_\emptyset < \tau_\mathrm{o}$) [9]. Due to this modification, the pole radii of the second network are moved closer to the unit circle, while their angles remain the same. The envelope $e_{\text{double}}(t)$ is turned into a double exponential curve, which exhibits the desired fade-in behaviour, see Figure 4.

$$h(t) = e^{-\frac{t}{\tau_\mathrm{o}}} e^{\imath\omega t} - e^{-\frac{t}{\tau_\emptyset}} e^{\imath\omega t} \tag{7}$$

$$= \left[e^{-\frac{t}{\tau_\mathrm{o}}} - e^{-\frac{t}{\tau_\emptyset}}\right] e^{\imath\omega t} \tag{8}$$

$$= e_{\text{double}}(t) e^{\imath\omega t}. \tag{9}$$

Note that the modal index i was omitted. This equation and all following ones apply to all modes of the network.

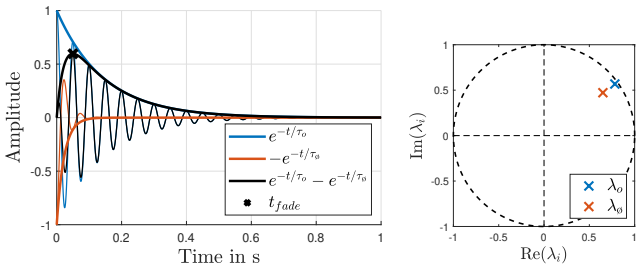

(a) Time Response and resulting envelope. (b) Poles.

Figure 4: Modes and resulting envelope for fade-in through modified pole radius. t_{fade} is defined as the maximum of the resulting envelope e_{double}.

We now derive the important equations which allow choosing the fade-in time according to some specification, for example according to a mixing time of a recorded impulse response [14]. In a hybrid reverb application, the fade-in time will correspond to the time after which no more image sources are calculated. The "fade-in time" t_{fade} will be defined as the maximum point of the curve and can be determined from the two time-constants as

$$t_{\text{fade}} = \log\left(\frac{\tau_o}{\tau_\emptyset}\right)\frac{\tau_o\tau_\emptyset}{\tau_o - \tau_\emptyset}. \tag{10}$$

When the reverberation time is given, the task is to find the correct time constants to achieve a given t_{fade}. To find the time constant, Equation 10 has to be solved for $\tau_\emptyset$. This is done using the lower branch of the Lambert-W function, which is the inverse function of $f(x) = xe^x$, see appendix.

$$\tau_\emptyset = -\frac{t_{\text{fade}}}{W_{-1}\left(-\frac{t_{\text{fade}}}{\tau_o}e^{-\frac{t_{\text{fade}}}{\tau_o}}\right)} \tag{11}$$

Figure 5 shows how the second time constant should be chosen depending on the first. Using this method, the fade-in time can not be placed at an arbitrary position, but the longest possible time depends on the desired T_{60}. If the time constant of the second network asymptotically approaches the first,

$$\hat{t}_{\text{fade}} = \lim_{\tau_\emptyset \to \tau_o} \log\left(\frac{\tau_o}{\tau_\emptyset}\right)\frac{\tau_o\tau_\emptyset}{\tau_o - \tau_\emptyset} \tag{12}$$

$$= \lim_{\tau_\emptyset \to \tau_o} -\log\left(\frac{\tau_o}{\tau_\emptyset}\right)\tau_o + \tau_o = \tau_o, \tag{13}$$

the maximal fade-in time $\hat{t}_{\text{fade}}$ is found to be equal to τ_o. This means that the fade-in time may approach approximately $\frac{T_{60}}{6.9078}$, which corresponds to about 14.4% of the desired reverberation time T_{60}. An example of an FDN response with the described fade-in behaviour is shown in Fig. 7.

By the nature of the double exponential decay, the output level of the FDN will decrease with increasing fade-in time, also see Figure 6. In the limit case of eq. 13, in which both networks are equal, there would in fact be no output at all. This loss in level should be compensated for, such that the fade-in time can be adjusted, while maintaining a sufficient output level. The maximal

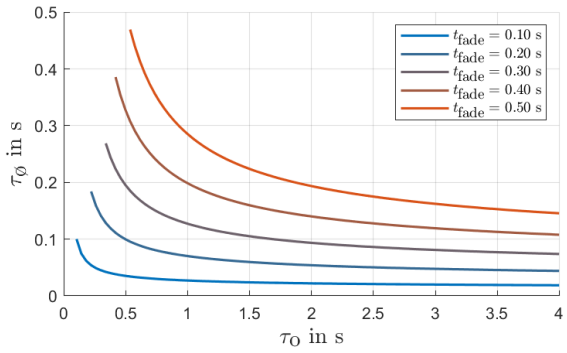

Figure 5: Relation between τ_o and $\tau_\emptyset$ for different constant t_{fade} values. The curve values are only valid for $t_{\text{fade}} < \tau_o$. Please note that for a constant fade-in time, longer τ_o requires a shorter $\tau_\emptyset$.

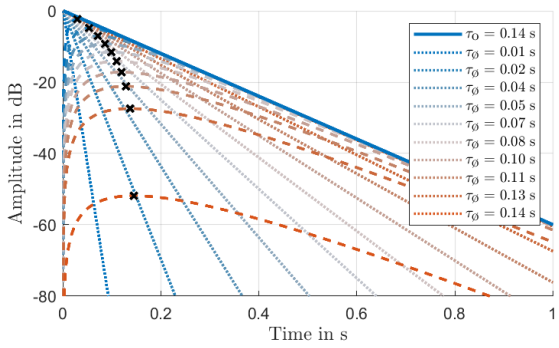

Figure 6: Signal envelope for constant reverberation time with τ_o (solid line) and varying $\tau_\emptyset$ (dotted lines). The difference envelope is indicated by the dashed lines, whereas the maxima are the resulting fade-in times t_{fade} are indicated with $\times$.

value of the envelope value found at the fade-in time can be used for normalization

$$e_{\text{double}}(t_{\text{fade}}) = \left(\frac{\tau_\emptyset}{\tau_o}\right)^{\frac{\tau_\emptyset}{(\tau_o - \tau_\emptyset)}} - \left(\frac{\tau_\emptyset}{\tau_o}\right)^{\frac{\tau_o}{(\tau_o - \tau_\emptyset)}}. \tag{14}$$

3.2. Frequency Dependent Double Decay

If filters are applied in the feedback path in order to obtain a frequency dependent reverberation time $T_{60}(\omega)$, the filter-gains have to be adjusted according to Eq. 6. Graphic Equalizers can be used in the feedback paths to obtain precise control over the frequency dependent reverberation time [15], but care has to be taken with respect to the filter design, as the recursive structure will amplify errors [16]. In most cases, the reverberation time should be frequency-dependent, but in regular applications, the fade-in time should be the same for all frequencies. This means that the second time constant needs to be different in every frequency band as well. In Section 3.4, we also show pole differences in a network with reverberation time control in two frequency bands.

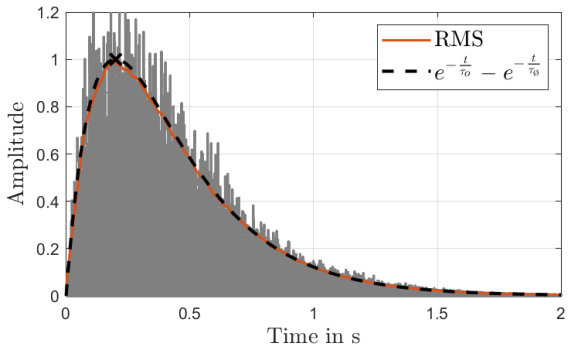

Figure 7: Absolute value of an FDN response, and its normalized RMS value along with the computed envelope.

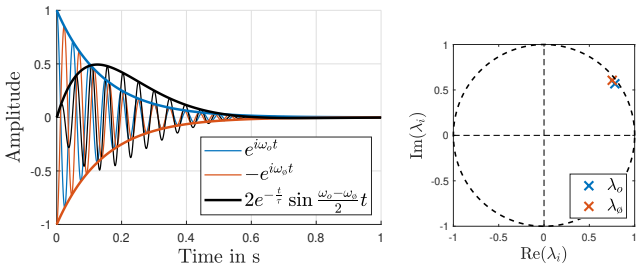

(a) Time Response and resulting envelope. (b) Poles.

Figure 8: Fade-in behaviour due to modified pole frequency. The resulting envelope is the first half-wave of a sinusoid, attenuated by exponential decay.

3.3. Modal Beating

Network size against echo and modal densities are the central trade-offs that needs to be negotiated in any FDN design [17]. The double decay approach, however, has the main disadvantage that the second FDN ø doesn't contribute to density at all.

Another option for realizing fade-in behaviour is to keep the attenuation gains of the second network equal to the first, and instead introduce a slight modification of the feedback matrix $\boldsymbol{A}_\text{ø}$. We have found that a small rotation yields the best results

$$\boldsymbol{A}_\text{ø} = \boldsymbol{A}_\text{o}\boldsymbol{R}, \tag{15}$$

where $\boldsymbol{R}$ is a rotation matrix close to the identity matrix. During the first few iterations, the network output is cancelled out just as in the double decay approach, but after a sufficient number of iterations, the output signals become different. Thus, in contrast to the double decay approach, both FDNs o and ø contribute equally to the late tail, doubling the modal and echo density of the complete system.

The rotated feedback matrix $\boldsymbol{A}_\text{ø}$ results in modified frequencies of the poles ω_i. This difference does not lead to the double exponential envelope seen before, but to modal beating, i.e. the modal envelopes are modulated at the difference frequency of the

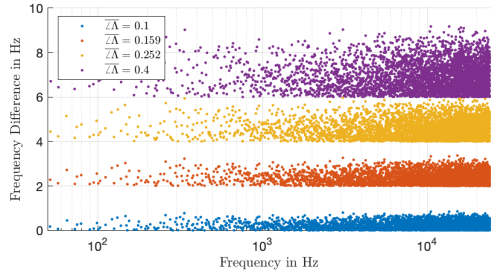

(a) Frequency difference of poles

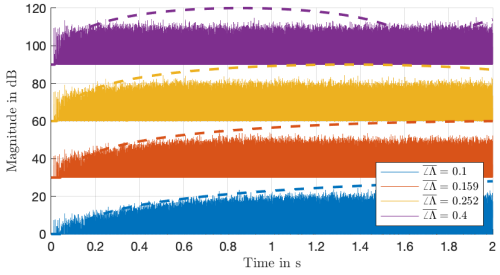

(b) Difference impulse responses

Figure 9: Fade-in behaviour due to modified pole frequency. The plots are offset by 2 Hz or 30 dB for better visualization, respectively. Only the behaviour of networks with moderate rotations (or long fade-in times) are described well by the mean pole rotation angle.

original and rotated pole

$$h(t) = e^{-\frac{t}{\tau}}e^{\imath\omega_\text{o}t} - e^{-\frac{t}{\tau}}e^{\imath\omega_\text{ø}t} \tag{16}$$

$$= 2e^{-\frac{t}{\tau}}\sin\left(\frac{\omega_\text{o}-\omega_\text{ø}}{2}t\right)e^{\imath\frac{\omega_\text{o}+\omega_\text{ø}}{2}t+\imath\pi} \tag{17}$$

$$= e_\text{beat}(t)e^{\imath\frac{\omega_\text{o}+\omega_\text{ø}}{2}t+\imath\pi}, \tag{18}$$

where the sine component indicates the beating envelope $e_\text{beat}(t)$. If the frequency shift is small enough, the first period of the modulation serves as fade-in. Fig. 8 depicts the beating of two modes with small difference and the corresponding pole positions.

As the rotation of an orthogonal matrix yields another orthogonal matrix, the magnitudes of the poles do not vary between the two FDNs. However, the rotation of the feedback matrix is not related to a rotation of the poles in a simple manner. In fact, typically each pole angle is modified differently. Thus, while the initial fade-in of the modal beating is in unison, the many different frequencies create a dense response for the subsequent beating periods. We define a mean beating frequency

$$\overline{\omega} = \frac{1}{\mathfrak{N}}\sum_{i=1}^{\mathfrak{N}}\frac{\omega_{\text{o},i}-\omega_{\text{ø},i}}{2}. \tag{19}$$

Fig. 9 shows an example of four lossless fade-in FDNs with varying matrix modification. Fig. 9a shows the pole frequency differences for each of the fade-in FDNs. Fig. 9b depicts the corresponding impulse response with the fade-in envelope determined from the mean beating frequencies $\overline{\omega}$.

In the following, we present a simple statistical relation between the rotation matrix and the resulting shift in pole angles. We

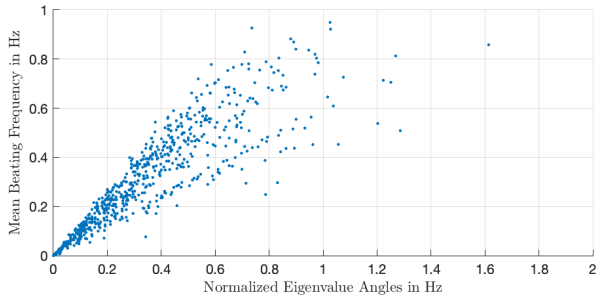

Figure 10: Relation between mean frequency difference and rotation matrix eigenvalue angle.

choose the rotation matrix such that for the eigenvalue decomposition

$$\boldsymbol{R} = \boldsymbol{Q}^{-1}\boldsymbol{\Lambda}\boldsymbol{Q} \tag{20}$$

the eigenvectors $\boldsymbol{Q}$ are also eigenvectors of $\boldsymbol{A}_\text{o}$ and the eigenvalue angles are of equal magnitude, i.e.,

$$|\angle\Lambda_{ii}| = \overline{\angle\Lambda} \text{ for any } 1 \leq i \leq N. \tag{21}$$

As a consequence, all eigenvalues of $\boldsymbol{A}_\text{ø}$ are rotated by a constant angle compared to $\boldsymbol{A}_\text{o}$. To determine the influence of the matrix rotation on the FDN poles, we perform a Monte Carlo experiment. We generated 500 FDNs with uniform distribution of $N \in [4, 8]$, $m_i \in [200, 2000]$ samples, $\overline{\angle\Lambda} \in [0, 2]$ Hz and random orthogonal matrices. For each instance, we apply the modal decomposition and compute the frequency difference of the poles. Fig. 10 shows the scatter plot of the resulting values. From statistical sampling, we can derive linear relation between rotation angle $\overline{\angle\Lambda}$ and the mean beating frequency $\overline{\omega}$, i.e.,

$$\overline{\omega} \approx \frac{\overline{\angle\Lambda}}{\mathfrak{N}}. \tag{22}$$

In particular, low amount of rotation yields relatively accurate estimates of the fade-in behavior, while strong rotations have a wider dispersion.

3.4. Examples

To evaluate the two principles, FDNs were created using the FDNtoolbox [12]. Numerical modal decomposition based on the Ehrlich Aberth Iteration method [13] reveals the actual modes of the systems. The fade-in time is set to $t_\text{fade} = 0.1s$. The base FDNs have the delays $\boldsymbol{m} = [622, 1855, 592, 1946, 1128, 1362, 1655, 1185]$ samples and an 8×8 random orthogonal feedback matrix.

Figure 12a shows a numerical example of the frequency-independent double-decay method, see e.g. Figure 4. As expected, the found poles of the two networks have the same frequencies, but different amplitudes. When using a crossover in the feedback paths, different reverberation times can be achieved for different frequency bands. In order to maintain the same fade-in times in all bands, the decay constant of the second network needs to be adjusted individually, which leads to different pole amplitudes, demonstrated in Figure 12b. A simple fourth order Linkwitz-Riley crossover was used. Also the modal beating method can be verified by means of numerical modal analysis. Figure 12c demonstrates the changed pole frequencies of the second network with respect to the first.

4. CONCLUSIONS

Two approaches for including fade-in behaviour in an FDN by subtracting the output of a second, modified network were presented. The proposed technique is computationally efficient, in particular for MIMO systems, as it does not require cancellation using convolutions with the early part.

The double decay approach allows for easy control over the fade-in time using the provided formulas, based on solving the double exponential decay with the Lambert-W function. The maximal fade-in time is approximately 14.4% of the targeted T_{60}. Furthermore, it was shown that the approach works in a network with frequency-dependent reverberation time.

The modal beating approach is based on introducing a small rotation to the feedback matrix of the second network, which is more efficient in achieving a high density with equal network size, but it is harder to control. This makes it less suitable for frequency-dependant reverberation. Modal decomposition has been used to explain both approaches. Sound examples using both approach can be found online, also applied to a hybrid model as mentioned in the introduction.[3] In the future, fade-in can be combined with other recent FDN developments, such as delay feedback matrices, direction-dependent design, and time-variation.

5. ACKNOWLEDGMENTS

The authors wish to thank Matthias Frank and Daniel Rudrich who asked Nils Meyer-Kahlen to figure out how to choose $\tau_\text{ø}$, while he was working for them in 2019. This research has received funding from the European Union's Horizon 2020 research and innovation programme under the Marie Skłodowska-Curie grant agreement No. 812719.

6. REFERENCES

[1] James Moorer, "About this reverberation business," *Computer Music Journal*, vol. 3, no. 2, Jan. 1985.

[2] Vesa Valimaki, Julian D. Parker, Lauri Savioja, Julius O. Smith, and Jonathan S. Abel, "Fifty Years of Artificial Reverberation," *IEEE Transactions on Audio, Speech, and Language Processing*, vol. 20, no. 5, pp. 1421–1448, July 2012.

[3] Thibaut Carpentier, Markus Noisternig, and Olivier Warusfel, "Hybrid reverberation processor with perceptual control," in *17th International Conference on Digital Audio Effects*, 2014.

[4] Jont B. Allen and David A. Berkley, "Image method for efficiently simulating small-room acoustics," *The Journal of the Acoustical Society of America*, vol. 65, no. 4, pp. 943–950, 1979.

[5] Matthias Frank, Daniel Rudrich, and Manuel Brandner, "Augmented Practice-Room - Augmented Acoustics in Music Education," in *Fortschritte der Akustik - DAGA*, 2020, submitted.

[6] Rebecca Stewart and Damian Murphy, "A Hybrid Artificial Reverberation Algorithm," in *122nd AES Convention*, 2007.

[3] `http://research.spa.aalto.fi/publications/papers/dafx20-fadefdn/`

[7] Aaron B. Greenblatt, Jonathan S. Abel, and David P. Berners, "A hybrid reverberation crossfading technique," in *International Conference on Acoustics Speech and Signal Processing (ICASSP)*. Apr. 2010, IEEE.

[8] Franz Zotter and Matthias Frank, "Signal flow and effects in ambisonic productions," in *Ambisonics - A Practical 3D Audio Theory for Recording, Studio Production, Sound Reinforcement, and Virtual Reality*, pp. 99–129. Springer, Heidelberg, Germany, first edition, 2019.

[9] Esa Piirilä, Tapio Lokki, and Vesa Välimäki, "Digital signal processing techniques for non-exponentially decaying reverberation," in *Proceedings of the 1998 Digital Audio Effects Workshop (DAFX'98)*, Nov. 1998, pp. 21–24.

[10] Keun Sup Lee and Jonathan S Abel, "A Reverberator with Two-Stage Decay and Onset Time Controls," in *AES 129th Convention*, 2010.

[11] Christian Borß, *An Improved Parametric Model for the Design of Virtual Acoustics and its Applications*, Phd thesis, Ruhr-Universität Bochum, 2011.

[12] Sebastian J. Schlecht, "FDNTB: The feedback delay network toolbox," in *Proceedings of the 23rd International Conference on Digital Audio Effects (DAFx-20)*, 2020.

[13] Sebastian J. Schlecht and Emanuël A. P. Habets, "Modal Decomposition of Feedback Delay Networks," *IEEE Transactions on Signal Processing*, vol. 67, no. 20, pp. 5340–5351, Oct. 2019, arXiv: 1901.08865.

[14] Helena Peić Tukuljac, Ville Pulkki, Hannes Gamper, Keith Godin, Ivan J. Tashev, and Nikunj Raghuvanshi, "A Sparsity Measure for Echo Density Growth in General Environments," 2019, vol. 00 of *ICASSP 2019 - 2019 IEEE International Conference on Acoustics, Speech and Signal Processing (ICASSP)*, pp. 1 – 5.

[15] Karolina Prawda, Sebastian J Schlecht, and Vesa Välimäki, "Improved Reverberation Time Control for Feedback Delay Networks," 2019, Proc. Int. Conf. Digital Audio Effects (DAFx), pp. 1 – 7.

[16] Sebastian J Schlecht and Emanuël A P Habets, "Accurate reverberation time control in feedback delay networks," 2017, Proc. Int. Conf. Digital Audio Effects (DAFx), pp. 337 – 344.

[17] Sebastian J. Schlecht and Emanuel A. P. Habets, "Dense Reverberation with Delay Feedback Matrices," in *2019 IEEE Workshop on Applications of Signal Processing to Audio and Acoustics (WASPAA)*, New Paltz, NY, USA, Oct. 2019, pp. 150–154, IEEE.

[18] Jean-Marc Jot; Antoine Chaigne, "Digital delay networks for designing artificial reverberators," in *90th AES Convention*, 1991.

[19] Matthias Frank, Franz Zotter, and Alois Sontacchi, "Producing 3D Audio in Ambisonics," in *AES 57th International Conference*, 2015.

[20] John Stautner and Miller Puckette, "Designing Multi-Channel Reverberators," *Comput. Music J.*, vol. 6, no. 1, pp. 52 – 65, 1982.

7. APPENDIX: DERIVATIONS

Second Network's Time Constant: Derivation of Eq. (11) with the Lambert-W function, see Fig. 11.

$$t_{\text{fade}} = \log\left(\frac{\tau_\text{o}}{\tau_\text{ø}}\right)\frac{\tau_\text{o}\tau_\text{ø}}{\tau_\text{o}-\tau_\text{ø}} \tag{23}$$

$$t_{\text{fade}}\frac{\tau_\text{o}-\tau_\text{ø}}{\tau_\text{o}\tau_\text{ø}} = \log\left(\frac{\tau_\text{o}}{\tau_\text{ø}}\right) \tag{24}$$

$$e^{t_{\text{fade}}\frac{\tau_\text{o}-\tau_\text{ø}}{\tau_\text{o}\tau_\text{ø}}} = \frac{\tau_\text{o}}{\tau_\text{ø}} \tag{25}$$

$$\frac{1}{\tau_\text{o}}e^{-\frac{t_{\text{fade}}}{\tau_\text{o}}} = \frac{1}{\tau_\text{ø}}e^{-\frac{t_{\text{fade}}}{\tau_\text{ø}}} \tag{26}$$

$$-\frac{t_{\text{fade}}}{\tau_\text{o}}e^{-\frac{t_{\text{fade}}}{\tau_\text{o}}} = -\frac{t_{\text{fade}}}{\tau_\text{ø}}e^{-\frac{t_{\text{fade}}}{\tau_\text{ø}}} \tag{27}$$

$$W_{-1}(-\frac{t_{\text{fade}}}{\tau_\text{o}}e^{-\frac{t_{\text{fade}}}{\tau_\text{o}}}) = \frac{t_{\text{fade}}}{\tau_\text{ø}} \tag{28}$$

$$\tau_\text{ø} = -\frac{t_{\text{fade}}}{W_{-1}(-\frac{t_{\text{fade}}}{\tau_\text{o}}e^{-\frac{t_{\text{fade}}}{\tau_\text{o}}})} \tag{29}$$

Maximum Fade-in Time: Derivation of Eq. (12)

$$\hat{t}_{\text{fade}} = \lim_{\tau_\text{ø}\to\tau_\text{o}} \log(\frac{\tau_\text{o}}{\tau_\text{ø}})\frac{\tau_\text{o}\tau_\text{ø}}{\tau_\text{o}-\tau_\text{ø}} \tag{30}$$

$$= \lim_{\tau_\text{ø}\to\tau_\text{o}} \frac{d(\log(\frac{\tau_\text{o}}{\tau_\text{ø}})\tau_\text{o}\tau_\text{ø})/d\tau_\text{ø}}{d(\tau_\text{o}-\tau_\text{ø})/d\tau_\text{ø}} \tag{31}$$

$$= \lim_{\tau_\text{ø}\to\tau_\text{o}} \frac{-\frac{1}{\tau_\text{ø}}\tau_\text{o}\tau_\text{ø} + \log(\frac{\tau_\text{o}}{\tau_\text{ø}})\tau_\text{o}}{-1} \tag{32}$$

$$= \lim_{\tau_\text{ø}\to\tau_\text{o}} \tau_\text{o} - \log(\frac{\tau_\text{o}}{\tau_\text{ø}})\tau_\text{o} = \tau_\text{o} \tag{33}$$

Envelope due to modified pole frequency: Derivation of Eq. (16)

$$h(t) = e^{-\frac{t}{\tau}}e^{\imath\omega_\text{o}t} - e^{-\frac{t}{\tau}}e^{\imath\omega_\text{ø}t} \tag{34}$$

$$= e^{-\frac{t}{\tau}}\left[e^{\imath\omega_\text{o}t} - e^{\imath\omega_\text{ø}t}\right] \tag{35}$$

$$= e^{-\frac{t}{\tau}}e^{\imath\frac{\omega_\text{o}+\omega_\text{ø}}{2}t}[e^{\imath\frac{\omega_\text{o}-\omega_\text{ø}}{2}t} - e^{\imath\frac{\omega_\text{ø}-\omega_\text{o}}{2}t}] \tag{36}$$

$$= e^{-\frac{t}{\tau}}e^{\imath\frac{\omega_\text{o}+\omega_\text{ø}}{2}t}2\imath\sin\left(\frac{\omega_\text{o}-\omega_\text{ø}}{2}t\right) \tag{37}$$

$$= 2e^{-\frac{t}{\tau}}\sin\left(\frac{\omega_\text{o}-\omega_\text{ø}}{2}t\right)e^{\imath\frac{\omega_\text{o}+\omega_\text{ø}}{2}t+\imath\pi} \tag{38}$$

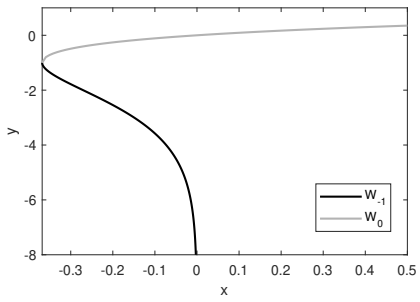

Figure 11: Lambert-W function for branches -1 and 0.

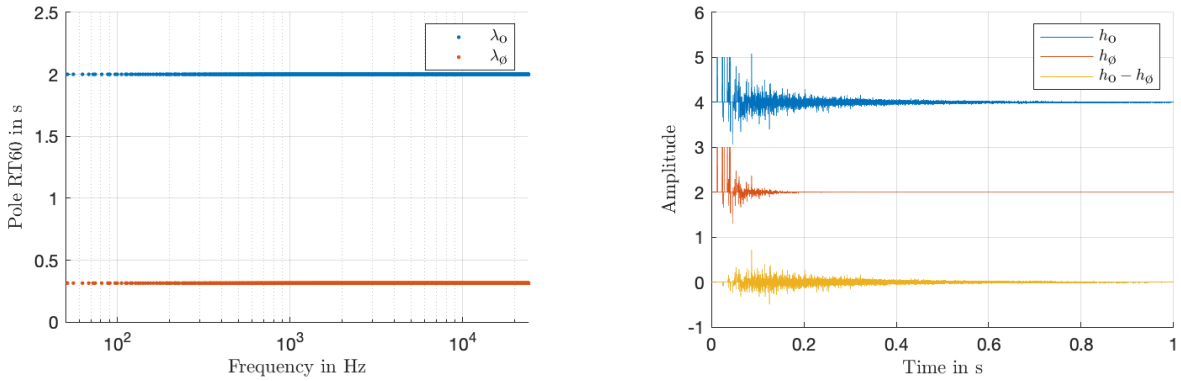

(a) Frequency-Independent Double Decay

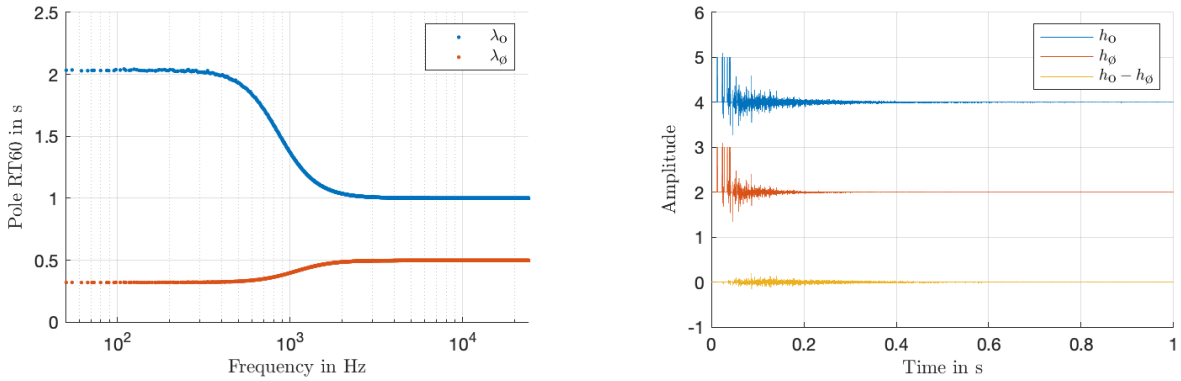

(b) Frequency-Dependent Double Decay

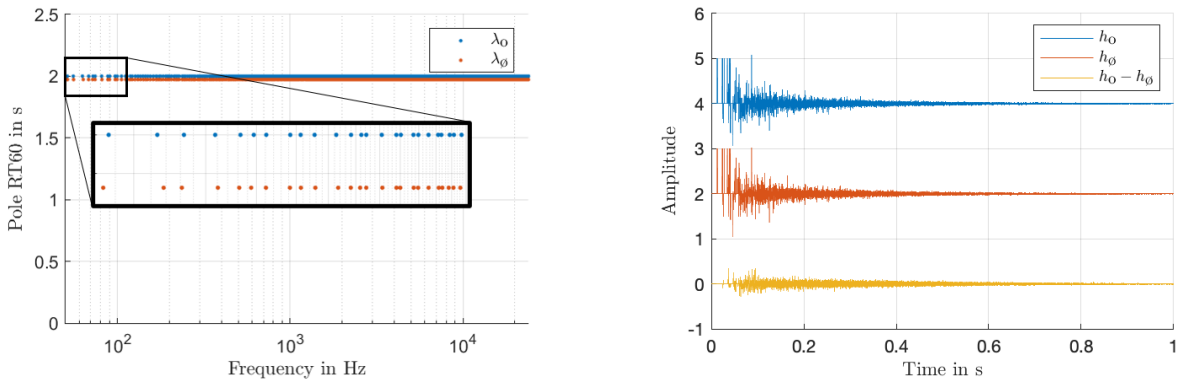

(c) Modal Beating

Figure 12: Numerical examples of fade-in FDN pole distribution and impulse responses. The left column shows the reverberation time of the poles of the o and ø. The right column shows the impulse responses of the individual FDNs o and ø and their difference, which shows the fade-in behaviour. The fade-in time is set to $t_{\text{fade}} = 0.1s$. The base FDNs have the delays $\boldsymbol{m} = [622, 1855, 592, 1946, 1128, 1362, 1655, 1185]$ samples and an 8×8 random orthogonal feedback matrix.